

Hints for multiple populations in intermediate-age clusters of the Small Magellanic Cloud

ANDRÉS E. PIATTI^{1,2}

¹*Consejo Nacional de Investigaciones Científicas y Técnicas, Av. Rivadavia 1917, C1033AAJ, Buenos Aires, Argentina*

²*Observatorio Astronómico de Córdoba, Laprida 854, 5000, Córdoba, Argentina*

Submitted to AJ

ABSTRACT

We report on the magnitude of the intrinsic [Fe/H] spread in the Small Magellanic Cloud (SMC) intermediate-age massive clusters NGC 339, 361, Lindsay 1 and 113, respectively. In order to measure the cluster metallicity dispersions, we used accurate Strömgren photometry of carefully selected cluster red giant branch (RGB) stars. We determined the Fe-abundance spreads by employing a maximum likelihood approach. The spreads obtained using the more accurate photometry of the brighter RGB stars resulted to be marginal ($\sim 0.05 \pm 0.03$ dex) for NGC 339 and NGC 361, while for Lindsay 1 and Lindsay 113 we obtained metallicity spreads of 0.00 ± 0.04 dex. From these results, we speculated with the possibility that NGC 361 is added to the group of four SMC clusters with observational evidence of multiple populations (MPs). Furthermore, in the context of the present debate about the existence of Fe-abundance inhomogeneities among old clusters with MPs, these outcomes put new constraints to recent theoretical speculations for making this phenomenon visible.

Keywords: techniques: photometric — galaxies: individual: SMC — Magellanic Clouds.

1. INTRODUCTION

Four intermediate-age (5–8 Gyr) massive ($\gtrsim 10^5 M_\odot$) clusters of the Small Magellanic Cloud (SMC) have been found to harbour multiple stellar populations (Kron 3, Lindsay 1, NGC 339 and 416 [Hollyhead et al. 2018](#)); to which other fourteen may also be added to the list of suitable targets for multiple population (MP) searches, namely: Lindsay 38 ([Piatti et al. 2001](#)), Lindsay 110, 112, 113 ([Piatti et al. 2007](#)), NGC 361 ([Mighell et al. 1998](#)), AM 3, HW 40, 41, 42, 59, 63 ([Piatti 2011a](#)), HW 22 ([Piatti 2011b](#)), ESO 51-SC9 ([Piatti 2012](#)) and BS 196 ([Bica et al. 2008](#)). A common feature that arises from Kron 3 ([Hollyhead et al. 2018](#)) and Lindsay 1 ([Hollyhead et al. 2017](#)) spectroscopic analyses is that the clusters show spreads in the abundances of light elements, a characteristic commonly seen in old globular clusters. For NGC 339 and NGC 416 [Niederhofer et al. \(2017\)](#) obtained *HST* UV/optical data from which difference in the abundance of N can be inferred. As far as we are aware, there is no study to seek for variation in Fe-abundances ([Fe/H]) in these SMC clusters.

The existence of [Fe/H] intrinsic spread among Milky Way globular clusters with observed MPs seems to be a feature of a very small minority. Only 8 Milky Way old globular clusters out of a population of 156 ([Harris 1996](#)) have inhomogeneities in [Fe/H] > 0.05 dex ([Johnson et al. 2015](#); [Marino et al. 2015](#)). Among the 15 known Large Magellanic Cloud old globular clusters, only NGC 1754, 2210, and 2257 have been searched for anomalies in their metallicities by [Mucciarelli et al. \(2009a\)](#), who concluded from [Fe/H] values of 5–7 stars per globular cluster that they exhibit quite homogeneous iron abundances (intrinsic spread = 0.02–0.04 dex) despite the observed occurrence of light element variations such as an Na–O anti-correlation. Therefore, they show very similar properties to the vast majority of Galactic globular clusters. From this perspective, anomalies in the iron content would not appear to be the most frequent manifestation of the globular cluster MPs formation, as recently reviewed by [Bastian & Lardo \(2017\)](#).

From a theoretical point of view, different models have recently proposed distinct scenarios to describe abundance anomalies in a variety of chemical elements in massive clusters harboring MPs. For instance, Bekki & Tsujimoto (2016)’s model is based on merger events, Bekki (2017) and Kim & Lee (2018) used supernovae enrichment and asymptotic giant branch star ejecta, while Gieles et al. (2018) proposed a concurrent formation of globular clusters and supermassive stars, among others.

These models have been mainly stimulated by observational findings of (anti-)correlations between chemical abundances of certain light elements (e.g., Na-O, Mg-Al, Mg-Si, Si-Zn; Osborn 1971; Cohen 1978; Carretta et al. 2009; Gratton et al. 2012; Hanke et al. 2017) and bimodalities in CN and CH that trace light element variations (e.g. Kayser et al. 2008; Martell & Grebel 2010, and references therein). Some of the models also propose mechanisms to obtain intrinsic [Fe/H] spreads > 0.05 dex. For instance, Gavagnin et al. (2016)’s model used merger events, while that of Bailin (2018) is based on feedback from core-collapse supernovae. Recently, Lim et al. (2017) found that globular clusters with large intrinsic [Fe/H] spreads also show a positive CN-CH correlation.

As Fe-abundance spread is considered, a frequent idea relies on the formation by merger events of two massive clusters with initially different [Fe/H], although there are still puzzling observational results which need to be addressed. Gavagnin et al. (2016) showed that the key parameters are the initial mass and density ratios of the progenitors. For instance, they found that the radial distributions of MPs in ω Cen and NGC 1851 are matched if the less massive progenitor are four times as dense as the larger one. The cluster’s mass has also been assumed to be a driver for such a metallicity inhomogeneity, in the sense that massive clusters ($> 10^7 M_{\odot}$) could inhibit the formation of second generation of stars with [Fe/H] by more than 0.05 dex larger than that for the first generation, because of SN feedback effects in the molecular clouds out of which globular clusters are formed (Bekki 2017). Indeed, the least massive Milky Way globular cluster ESO 452-SC11 ($M = 6.8 \pm 3.4 \times 10^3 M_{\odot}$ Simpson et al. 2017) does show MPs of stars each with a different chemical composition.

In this work we made use of Strömgren photometry of the SMC intermediate-age massive ($\gtrsim 10^5 M_{\odot}$ McLaughlin & van der Marel 2005a; Glatt et al. 2011) clusters NGC 339, 361, Lindsay 1 and 113 with the aim of investigating their metallicity distributions. The Strömgren photometric system has resulted to be very efficient at identifying MPs in globular clusters (Massari et al. 2016; Gruyters et al. 2017). Its medium-bandwidth filters has the advantage of allowing us to obtain accurate [Fe/H] values for many stars in a cluster field, straightforwardly, provided the photometric data are precise. Particularly, Frank et al. (2015) employed Strömgren metallicity-sensitive indices of stars located in the field of the peculiar Milky Way globular cluster NGC 2419 and found an Fe-abundance normal spread. Nevertheless, it should be noticed that with only the Strömgren m_1 index is not possible to distinguish between the presence of an iron and a light-element spread, or only a light-element spread.

The paper is organized as follows: Section 2 describes the data set employed and thoroughly establishes its accuracy. In Section 3 we derive individual [Fe/H] values for cluster stars paying particular attention to the estimation of the metallicity uncertainties, while Section 4 deals with the cluster metallicity distributions. Finally, Section 5 summarizes the main conclusions of this work.

2. OBSERVATIONAL DATA

The data used here were downloaded from the National Optical Astronomy Observatory (NOAO) Science Data Management (SDM) Archives¹, and are part of an observational campaign aiming at studying the age-metallicity relationships of Magellanic Clouds’ clusters (programme ID: SO2008B-0917, PI: Pietrzynski). They consist of Strömgren *vby* images of excellent quality (typical FWHM $\sim 0.6''$) obtained on the night of December 17, 2008, complemented with calibration and standard field images. They were taken with the SOAR Optical Imager (SOI) mounted on the 4.1m Southern Astrophysical Research (SOAR) telescope (FOV= $5.25' \times 5.25'$, scale= $0.154''/\text{px}$). We processed all the data set according to the recipes of the SOI pipeline².

To standardize our photometry we measured instrumental *vby* magnitudes of the standard stars TYC 7583-1011-1, 8104-856-1, 7548-698-1, 8104-820-1, HD 3417, 58489, 66020, and 57568 (Hauck & Mermilliod 1998; Paunzen 2015). Both Strömgren standard star compilations list for each star the Johnson *V* magnitude along with the $b - y$, m_1 , c_1 and β Strömgren indices. Here we used the *V* magnitude and the $b - y$ and m_1 color indices to fit the instrumental *vby* magnitudes, so that we obtained the standard ones by simply inverting the fitted relationships using the IRAF.PHOTCAL.INVERFIT task. Note that $m_1 = (v - b) - (b - y)$. The stars were observed at airmass between 1.02

¹ <http://www.noao.edu/sdm/archives.php>.

² <http://www.ctio.noao.edu/soar/content/soar-optical-imager-soi>

Table 1. Strömrgren transformation coefficients.

Filter	coef ₁	coef ₂	coef ₃	coef ₄	rms
<i>v</i>	1.137±0.027	0.301±0.016	2.008±0.058	1.028±0.068	0.017
<i>b</i>	0.959±0.003	0.163±0.002	0.942±0.003		0.002
<i>y</i>	0.946±0.015	0.118±0.009	-0.008±0.015		0.010

and 2.23 along the whole night. We then performed fits of the expressions:

$$v = v_1 + V_{\text{std}} + v_2 \times X_v + v_3 \times (b - y)_{\text{std}} + v_4 \times m_{1\text{std}},$$

$$b = b_1 + V_{\text{std}} + b_2 \times X_b + b_3 \times (b - y)_{\text{std}},$$

$$y = y_1 + V_{\text{std}} + y_2 \times X_y + y_3 \times (b - y)_{\text{std}},$$

using the IRAF.PHOTCAL.FITPARAMS routine where v_i , b_i and y_i are the i -th fitted coefficients, and X represents the effective airmass. Table 1 shows the resulting coefficients.

We obtained instrumental *vby* magnitudes of stars located in the four cluster fields using the stand-alone versions of DAOPHOT, ALLSTAR, DAOMATCH and DAOMASTER routine packages (Stetson et al. 1990). The magnitudes were derived from point-spread-function (PSF) fits performed using previously generated spatially quadratically varying PSFs. These PSFs were modeled from a sample of nearly 100 interactively selected stars distributed throughout the image, previously cleaned from fainter contaminating neighboring stars using a preliminary PSF built with nearly 40 relatively bright, well-isolated stars. Once we applied the resulting PSF to an image, we took advantage of the subtracted image to identify new fainter sources which were added to the final photometric catalog. In each of the three iterations performed, we did the PSF photometry for the whole sample of identified sources. Finally, we transformed the instrumental magnitudes into the Strömrgren photometric system using the coefficients listed in Table 1.

The quality of our photometry was first examined in order to obtain robust estimates of the photometric errors. To do this, we performed artificial star tests by using the stand-alone ADDSTAR program in the DAOPHOT package (Stetson et al. 1990) to add synthetic stars, generated bearing in mind the color and magnitude distributions of the stars in the color-magnitude diagram (CMD) - we were particularly interested in stars distributed along the cluster red giant branch (RGB) -, as well as the cluster radial stellar density profile. We added a number of stars equivalent to $\sim 5\%$ of the measured stars in order to avoid in the synthetic images significantly more crowding than in the original images. On the other hand, to avoid small number statistics in the artificial-star analysis, we created a thousand different images for each original one. We used the option of entering the number of photons per ADU in order to properly add the Poisson noise to the star images.

We then repeated the same steps to obtain the photometry of the synthetic images as described above, i.e., performing three passes with the DAOPHOT/ALLSTAR routines. The photometric errors were derived from the magnitude difference between the output and input data of the added synthetic stars using the DAOMATCH and DAOMASTER tasks. We found that this difference resulted typically equal to zero and in all the cases smaller than 0.003 mag. The respective rms errors were adopted as the photometric errors. Fig. 1 illustrates the behavior of these errors as a function of the distance from the cluster center for two different magnitude level, namely $V = 16.5$ mag and 18.5 mag, respectively. These magnitudes roughly correspond to the upper and lower limits of the cluster RGBs used in this work (see Figs. 2-5).

3. METALLICITY ESTIMATES

As for metallicity estimates of individual stars we used the semi-empirical calibration of the reddening free metallicity-sensitive index $m_{1,o}$, in turn based on the stars' $(v - y)_o$ colors, derived by Calamida et al. (2007). Particularly, we used the expression:

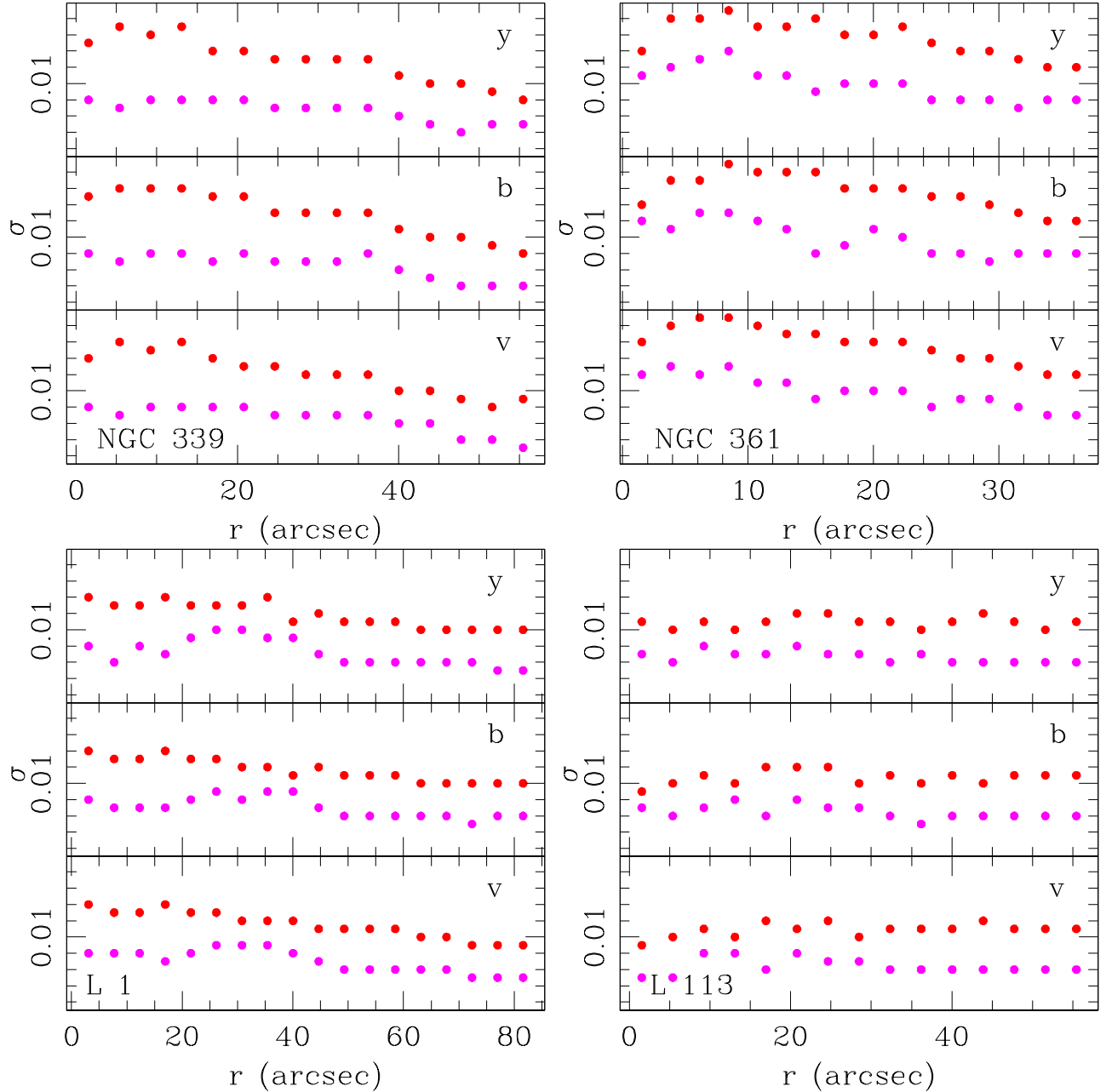


Figure 1. Photometric error estimates for the vby filters as a function of the distance to the cluster center. Magenta and red filled circles are for $V = 16.5$ and 18.5 mag, respectively.

$$m_{1o} = \alpha + \beta[\text{Fe}/\text{H}] + \gamma(v - y)_o + \delta[\text{Fe}/\text{H}](v - y)_o \quad (1)$$

where $\alpha = -0.309$, $\beta = -0.090 \pm 0.002$, $\gamma = 0.521 \pm 0.001$, and $\delta = 0.159 \pm 0.001$, respectively. We adopted the semi-empirical relation, since this is recommended by Calamida et al. (2007) as being the most robust for estimating the metallicity of red giants (see also Calamida et al. (2009); Adén et al. (2009); Árnadóttir et al. (2010); Frank et al. (2015)). Indeed, Piatti & Koch (2018) have recently obtained Strömgren-based $[\text{Fe}/\text{H}]$ values from 10 LMC ancient Large Magellanic Cloud globular clusters over a broad metallicity range ($-2.1 \leq [\text{Fe}/\text{H}] \text{ (dex)} \leq -1.0$) in excellent agreement with mostly high-dispersion spectroscopic values. Note that our derived mean cluster metallicities (see Table 2) are also in

excellent agreement with spectroscopic values). We provide in the Appendix a comparison of the $[\text{Fe}/\text{H}]$ values derived for selected stars (see below) from the semi-empirical calibration with those based on the empirical and theoretical ones, respectively. The reddening corrected m_{1o} and $(v-y)_o$ colors were obtained from the $E(m_1)$ and $E(v-y)$ color excesses computed using the $E(X)/E(B-V)$ ratios given by Crawford & Mandwewala (1976) and the $E(B-V)$ color excesses obtained from the NASA/IPAC Extragalactic Data base³ (NED) (see Table 2).

To estimate the uncertainties in the $[\text{Fe}/\text{H}]$ values, we performed a full analytical propagation of errors, including those on the calibration coefficients, as follows:

$$\sigma([\text{Fe}/\text{H}])^2 = \left(\frac{\partial[\text{Fe}/\text{H}]}{\partial\alpha}\sigma(\alpha)\right)^2 + \left(\frac{\partial[\text{Fe}/\text{H}]}{\partial\beta}\sigma(\beta)\right)^2 + \left(\frac{\partial[\text{Fe}/\text{H}]}{\partial\gamma}\sigma(\gamma)\right)^2 + \left(\frac{\partial[\text{Fe}/\text{H}]}{\partial\delta}\sigma(\delta)\right)^2 + \left(\frac{\partial[\text{Fe}/\text{H}]}{\partial m_{1o}}\sigma(m_{1o})\right)^2 + \left(\frac{\partial[\text{Fe}/\text{H}]}{\partial(v-y)_o}\sigma((v-y)_o)\right)^2,$$

$$\sigma([\text{Fe}/\text{H}])^2 = \left(\frac{0.002[\text{Fe}/\text{H}]}{c}\right)^2 + \left(\frac{0.001(v-y)_o}{c}\right)^2 + \left(\frac{0.001[\text{Fe}/\text{H}](v-y)_o}{c}\right)^2 + \left(\frac{\sigma(m_{1o})}{c}\right)^2 +$$

$$\left(\frac{(-0.521c - 0.159(m_{1o} + 0.309 - 0.521(v-y)_o)\sigma((v-y)_o))}{c^2}\right)^2$$

where $c = -0.090 + 0.159(v-y)_o$, and $\sigma(m_{1o})$ and $\sigma((v-y)_o)$ are the photometric errors in m_{1o} and $(v-y)_o$, respectively, according to the position of the stars with respect to the cluster's center (see Fig. 1).

We then carefully selected *bonafide* cluster members on the basis of the following criteria: i) they are located inside the clusters' radii (Hill & Zaritsky 2006; Glatt et al. 2009, 2011). ii) They are distributed along the RGBs above the respective red clumps/horizontal branches. The cluster RGBs in the V versus $b-y$ and V versus $v-y$ CMDs are not dominated by metallicity effects, so that they result in narrow star sequences. We traced the RGB ridge lines and discarded any stars with $b-y$ and $v-y$ colors that differ in more than 0.05 mag from those of the RGC ridge lines. In addition, the cluster RGBs are the least contaminated CMD features by field stars. Indeed, by using different field regions of equal cluster areas, distributed around the clusters, we found that the number of field stars that fall inside the RGB strips is smaller than 10 per cent with respect to the total number of adopted RGB cluster members. iii) They span the readily visible cluster $[\text{Fe}/\text{H}]$ range as judged by the dispersion (\sim within $2\times$ standard deviation) of $[\text{Fe}/\text{H}]$ values for the brightest selected stars, i.e., those drawn with magenta open circles in Figs. 2-5. In order to achieve this, we discarded some few stars that only satisfied criteria i and ii, but fall outside the aforementioned $[\text{Fe}/\text{H}]$ range. They are drawn with filled red circles in Figs. 2-5. Note that the brightest selected stars (magenta circles) are those with more accurate photometry, and hence with the smallest $[\text{Fe}/\text{H}]$ uncertainties. Likewise, as the V magnitude increases, both the metallicity errors and the dispersion of the individual $[\text{Fe}/\text{H}]$ values increase (see bottom-right panels of Figs. 2 to 5), because of the poorer photometry quality (see Fig. 1). For these reasons, the observed $[\text{Fe}/\text{H}]$ range of the brightest selected stars more properly reveals the cluster metallicity range. Because of this metallicity range should be the same at any magnitude level, we used it for discarding some few stars fainter than those marked with magenta circles. We simply included the stars with red circles with the purpose of enlarging the star sample, while the clusters' mean metallicities and dispersions keep unchanged from an astrophysical point of view with respect the values derived using only the brightest selected stars.

Figs. 2 to 5 show the resulting observed CMDs and the derived individual $[\text{Fe}/\text{H}]$ values with their respective uncertainties. Stars observed within the cluster areas and those for comparison star fields with equal cluster areas are depicted with filled black and green circles, while the selected stars are encircled with magenta and red open circles, respectively. As can be seen, the combination of an accurate photometry (see also Table 1 and Fig. 1) and an accurate metallicity calibration (see eq.(1)) resulted in an advantageous tool for estimating cluster RGB stars' metallicities with uncertainties that, in the case of the brightest objects, are of the same order than those expected from high-dispersion spectroscopy. For the sake of the reader we have also included the $v-y$ versus m_1 color-color diagrams in Fig. 6.

4. ANALYSIS AND DISCUSSION

In order to assess whether the metallicity distributions are shaped by the presence of an intrinsic spread in Fe-abundances, we derived the mean and dispersion of each cluster's Fe-abundance by employing a maximum likelihood approach. The relevance lies in accounting for individual star measurements, which could artificially inflate the dis-

³ <http://ned.ipac.caltech.edu/>. NED is operated by the Jet Propulsion Laboratory, California Institute of Technology, under contract with NASA.

persion if ignored. We optimized the probability \mathcal{L} that a given ensemble of stars with metallicities $[\text{Fe}/\text{H}]_i$ and errors σ_i are drawn from a population with mean Fe-abundance $\langle [\text{Fe}/\text{H}] \rangle$ and dispersion W (e.g., Pryor & Meylan 1993; Walker et al. 2006), as follows:

$$\mathcal{L} = \prod_{i=1}^N (2\pi(\sigma_i^2 + W^2))^{-\frac{1}{2}} \exp\left(-\frac{([\text{Fe}/\text{H}]_i - \langle [\text{Fe}/\text{H}] \rangle)^2}{2(\sigma_i^2 + W^2)}\right)$$

where the errors on the mean and dispersion were computed from the respective covariance matrices. Table 2 lists in the last columns all our results, where the W values refer to the selected N brightest stars (open magenta circles in Figs. 2-5). In case of using all the cluster RGB stars, W turns out to be equal to zero for all the clusters. This is a consequence of dealing with larger $[\text{Fe}/\text{H}]$ errors, since both groups of selected stars (brighter and fainter than a fixed V magnitude) span nearly the same metallicity range and have similar average metallicity values. Here, the larger individual $[\text{Fe}/\text{H}]$ errors of fainter stars blur any possible intrinsic spread.

Our findings show that among the two studied MP SMC clusters only NGC 339 exhibits a relatively small Fe-abundance dispersion. This result could imply that the intrinsic spread in metallicity is not a common feature in these MP SMC star clusters, as is not in Milky Way old globular clusters either, or that more accurate metal abundance estimates are required. In any case, the amount of metallicity spread would appear to be somehow marginal, i.e., smaller than the values found in eight Milky Way globular clusters (> 0.10 dex). Likewise, note also that we have not used some RGB stars that are located inside the clusters' radii, are placed along the cluster RGBs and have similar $[\text{Fe}/\text{H}]$ errors like those selected stars, which would enlarge the cluster metallicity range. In this sense, the Fe-abundance spreads found in this study should be considered as lower limits.

The Strömgen metallicities derived in this analysis come from measurements of the m_1 index = $(v - b) - (b - y)$ calibrated in terms of $[\text{Fe}/\text{H}]$ values obtained from high-dispersion spectroscopy. In this sense, Calamida et al. (2007) used the m_1 index as a photometric proxy for the iron abundance. However, the CN absorption band at 4142 Å is near to the effective wavelength of the v filter, so that the derived dispersions W could reflect variations in light-element abundances. Nevertheless, according to (Lim et al. 2017), globular clusters with heavy element abundance variations do show a CN-CH positive correlation, unlike normal globular clusters. In this sense, the derived $[\text{Fe}/\text{H}]$ values might reflect both heavy and light element abundances or only those from light elements. Further analyses with the Strömgen c_1 index or from spectroscopic data are needed.

For NGC 361 we obtained an W value similar to that for the MP SMC cluster NGC 339, from which we infer that the former could also be added to the list of SMC clusters harboring MPs. In the case of Lindsay 113, we cannot conclude on the existence of MPs, because of the lack of evidence of any small mean iron spread among the measured stars. Several theoretical models have recently proposed different scenarios to describe abundance anomalies in a variety of chemical elements in massive clusters with MPs (see, e.g. Bekki & Tsujimoto 2016; Bekki 2017; Bailin 2018; Gieles et al. 2018; ?, and references therein). They have been mainly stimulated by observational results of anti-correlations between chemical abundances of light elements, although some of the models also suggest mechanisms to obtain intrinsic $[\text{Fe}/\text{H}]$ spreads > 0.05 dex. Here we would like to mention that our studied clusters are more massive than the MP globular cluster ESO 452-SC11 ($M = 6.8 \pm 3.4 \times 10^3 M_\odot$) (see Table 2, for which Simpson et al. (2017) found difference in chemical compositions).

5. CONCLUSION

With the aim of investigating whether SMC intermediate-age clusters with light chemical abundance variations also shows Fe-abundance spreads, we conducted an analysis of NGC 339 and Lindsay 1, recently confirmed as MP SMC clusters. We also added NGC 361 and Lindsay 113, two SMC intermediate-age clusters with well-populated RGBs.

We made use of publicly available vby Strömgen images centered on these clusters, from which we obtained accurate photometric data sets. We extensively and carefully probed the precision of our photometry, focused on stars distributed along the cluster RGBs, for which we attained uncertainties smaller than 0.02 magnitudes in all the three filters, regardless the stars are located in the innermost or outermost regions of the clusters.

As the metallicity estimate is concerned, we employed a well-established, high-dispersion spectroscopy based calibration of the Strömgen metallicity-sensitive index m_1 . We derived individual $[\text{Fe}/\text{H}]$ values for RGB stars brighter than those placed at the cluster red clump/horizontal branch. For the brightest cluster RGC stars we estimated uncertainties comparable to those expected from precise spectroscopic observations. From these metallicity estimates we computed their mean and intrinsic dispersion. We obtained mean metal abundances in very good agreement

Table 2. Astrophysical properties of SMC clusters.

Cluster	$E(B - V)_{\text{NED}}$	Age	Ref.	$[\text{Fe}/\text{H}]_{\text{lit.}}$	Ref.	Mass	Ref.	$[\text{Fe}/\text{H}]$	W	N
	(mag)	(Gyr)		(dex)		($\times 10^5 M_{\odot}$)				
NGC 339	0.03	5.4 ± 1.0	1,2	-1.19 ± 0.10	4,5	0.8	8	-1.27 ± 0.03	0.04 ± 0.03	11
NGC 361	0.03	6.8 ± 0.5	6	-1.08 ± 0.10	5	2.0	8	-1.13 ± 0.03	0.06 ± 0.03	10
Lindsay 1	0.03	7.5 ± 0.5	1,6	-1.01 ± 0.10	5	2.0	7	-1.11 ± 0.02	0.00 ± 0.04	13
Lindsay 113	0.04	4.6 ± 1.0	3,6	-1.17 ± 0.10	4	—		-1.19 ± 0.03	0.00 ± 0.04	7

NOTE— Ref.: (1) Glatt et al. (2008); (2) Piatti (2011a); (3) Piatti et al. (2007); (4) Da Costa & Hatzidimitriou (1998); (5) Mucciarelli et al. (2009b); (6) Mighell et al. (1998); (7) Glatt et al. (2011); (8) McLaughlin & van der Marel (2005b).

with those previously derived from spectroscopic studies and small intrinsic Fe-abundance spreads in NGC 339 and NGC 361. From this results we speculated with the possibility of NGC 361 being the fifth SMC intermediate-age cluster with MPs. The lack of detection of significant metallicity spreads in the MP SMC cluster Lindsay 1 as well as in Lindsay 113 could be attributed to the fact that this is not a common phenomenon among MP star clusters, or we need even more accurate metallicity estimates in order to asses the cluster metallicity spread more reliably.

Based on observations obtained at the Southern Astrophysical Research (SOAR) telescope, which is a joint project of the Ministério da Ciência, Tecnologia, Inovações e Comunicações (MCTIC) do Brasil, the U.S. National Optical Astronomy Observatory (NOAO), the University of North Carolina at Chapel Hill (UNC), and Michigan State University (MSU). We thank the referee for the thorough reading of the manuscript and timely suggestions to improve it.

REFERENCES

- Adén, D., Feltzing, S., Koch, A., et al. 2009, *A&A*, 506, 1147, doi: [10.1051/0004-6361/200912718](https://doi.org/10.1051/0004-6361/200912718)
- Árnadóttir, A. S., Feltzing, S., & Lundström, I. 2010, *A&A*, 521, A40, doi: [10.1051/0004-6361/200913544](https://doi.org/10.1051/0004-6361/200913544)
- Bailin, J. 2018, ArXiv e-prints. <https://arxiv.org/abs/1807.01447>
- Bastian, N., & Lardo, C. 2017, ArXiv e-prints. <https://arxiv.org/abs/1712.01286>
- Bekki, K. 2017, *MNRAS*, 469, 2933, doi: [10.1093/mnras/stx982](https://doi.org/10.1093/mnras/stx982)
- Bekki, K., & Tsujimoto, T. 2016, *ApJ*, 831, 70, doi: [10.3847/0004-637X/831/1/70](https://doi.org/10.3847/0004-637X/831/1/70)
- Bica, E., Santos, Jr., J. F. C., & Schmidt, A. A. 2008, *MNRAS*, 391, 915, doi: [10.1111/j.1365-2966.2008.13942.x](https://doi.org/10.1111/j.1365-2966.2008.13942.x)
- Calamida, A., Bono, G., Stetson, P. B., et al. 2007, *ApJ*, 670, 400, doi: [10.1086/521424](https://doi.org/10.1086/521424)
- . 2009, *ApJ*, 706, 1277, doi: [10.1088/0004-637X/706/2/1277](https://doi.org/10.1088/0004-637X/706/2/1277)
- Carretta, E., Bragaglia, A., Gratton, R., & Lucatello, S. 2009, *A&A*, 505, 139, doi: [10.1051/0004-6361/200912097](https://doi.org/10.1051/0004-6361/200912097)
- Cohen, J. G. 1978, *ApJ*, 223, 487, doi: [10.1086/156284](https://doi.org/10.1086/156284)
- Crawford, D. L., & Mandwewala, N. 1976, *PASP*, 88, 917, doi: [10.1086/130046](https://doi.org/10.1086/130046)
- Da Costa, G. S., & Hatzidimitriou, D. 1998, *AJ*, 115, 1934, doi: [10.1086/300340](https://doi.org/10.1086/300340)
- Frank, M. J., Koch, A., Feltzing, S., et al. 2015, *A&A*, 581, A72, doi: [10.1051/0004-6361/201526555](https://doi.org/10.1051/0004-6361/201526555)
- Gavagnin, E., Mapelli, M., & Lake, G. 2016, *MNRAS*, 461, 1276, doi: [10.1093/mnras/stw1397](https://doi.org/10.1093/mnras/stw1397)
- Gieles, M., Charbonnel, C., Krause, M. G. H., et al. 2018, *MNRAS*, 478, 2461, doi: [10.1093/mnras/sty1059](https://doi.org/10.1093/mnras/sty1059)
- Glatt, K., Grebel, E. K., Sabbi, E., et al. 2008, *AJ*, 136, 1703, doi: [10.1088/0004-6256/136/4/1703](https://doi.org/10.1088/0004-6256/136/4/1703)
- Glatt, K., Grebel, E. K., Gallagher, III, J. S., et al. 2009, *AJ*, 138, 1403, doi: [10.1088/0004-6256/138/5/1403](https://doi.org/10.1088/0004-6256/138/5/1403)
- Glatt, K., Grebel, E. K., Jordi, K., et al. 2011, *AJ*, 142, 36, doi: [10.1088/0004-6256/142/2/36](https://doi.org/10.1088/0004-6256/142/2/36)
- Gratton, R. G., Carretta, E., & Bragaglia, A. 2012, *A&A Rv*, 20, 50, doi: [10.1007/s00159-012-0050-3](https://doi.org/10.1007/s00159-012-0050-3)
- Gruyters, P., Casagrande, L., Milone, A. P., et al. 2017, *A&A*, 603, A37, doi: [10.1051/0004-6361/201630341](https://doi.org/10.1051/0004-6361/201630341)
- Hanke, M., Koch, A., Hansen, C. J., & McWilliam, A. 2017, *A&A*, 599, A97, doi: [10.1051/0004-6361/201629650](https://doi.org/10.1051/0004-6361/201629650)

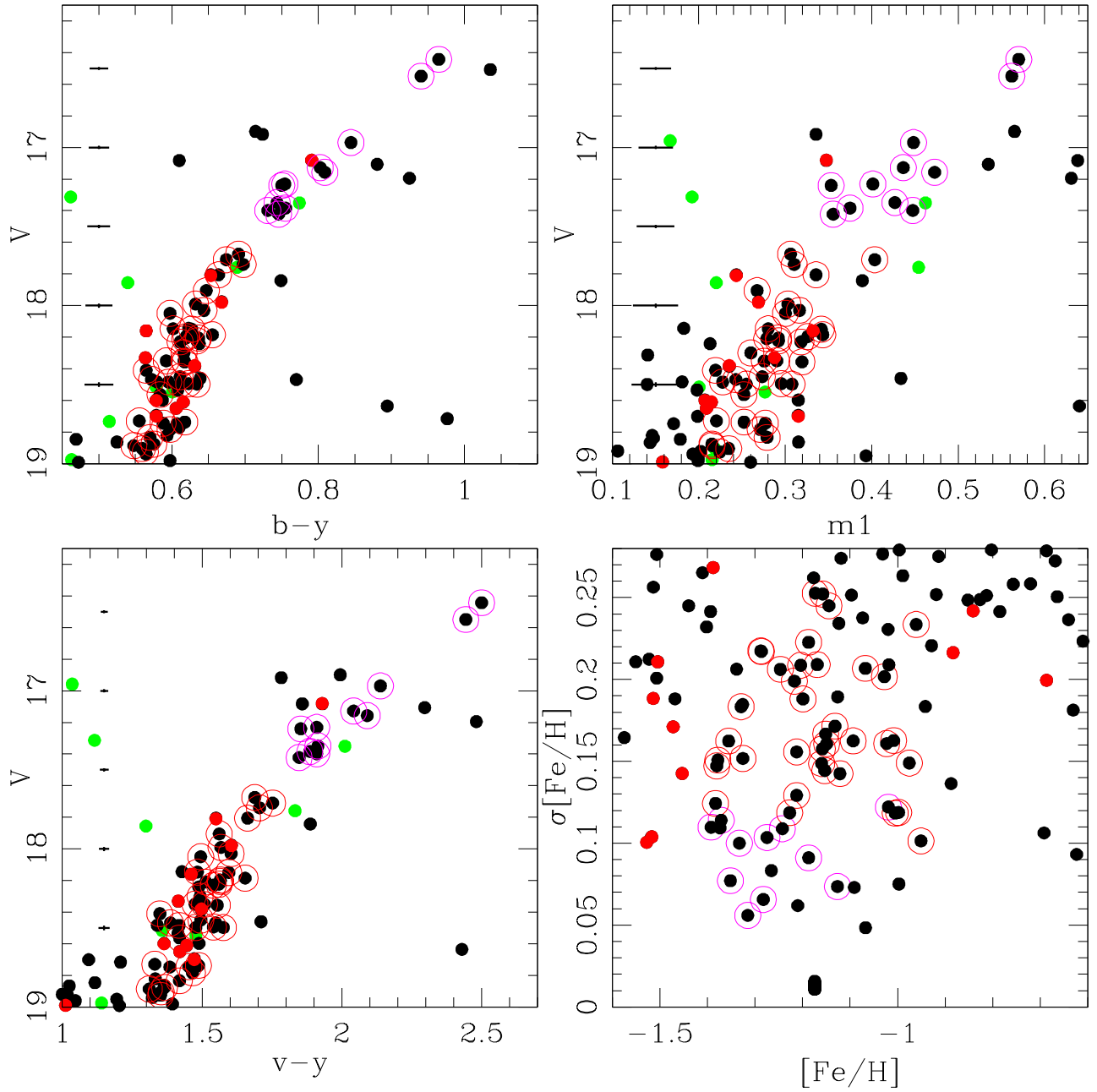


Figure 2. Observed CMDs of stars observed in the field of NGC 339. Black and green filled circles represent stars observed in the cluster area and in a comparison star field with an equal cluster area, respectively. Red filled circles represent stars that only satisfied the selection criteria i and ii (see text for details). Average error bars are also depicted at the left-hand margin of the CMDs. The individual metallicities ($[\text{Fe}/\text{H}]$) and their respective uncertainties are depicted in the bottom-right panel. We split the sample in brighter and fainter selected stars highlighted with magenta and red open circles, respectively.

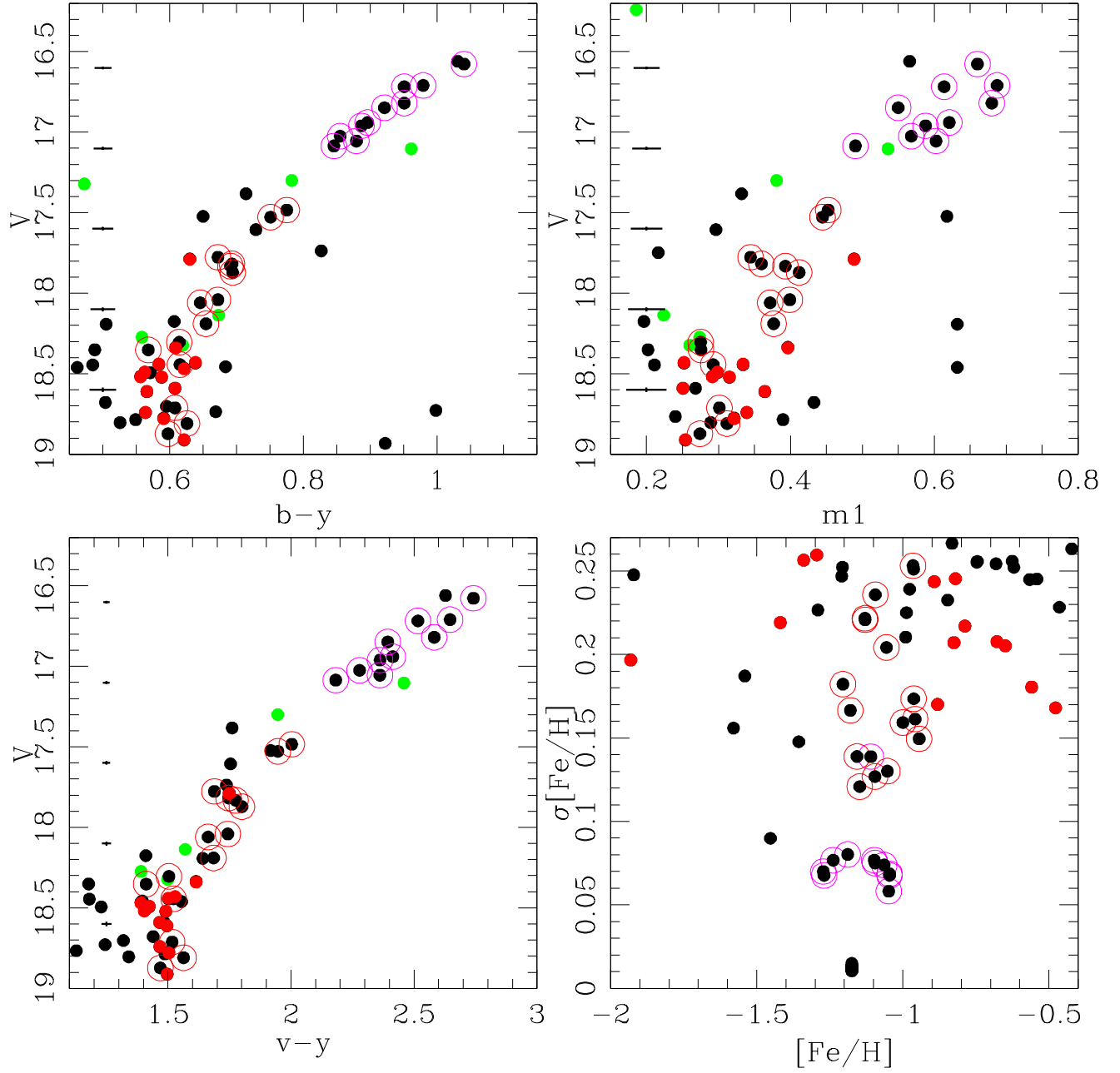


Figure 3. Same as Fig. 1 for NGC 361.

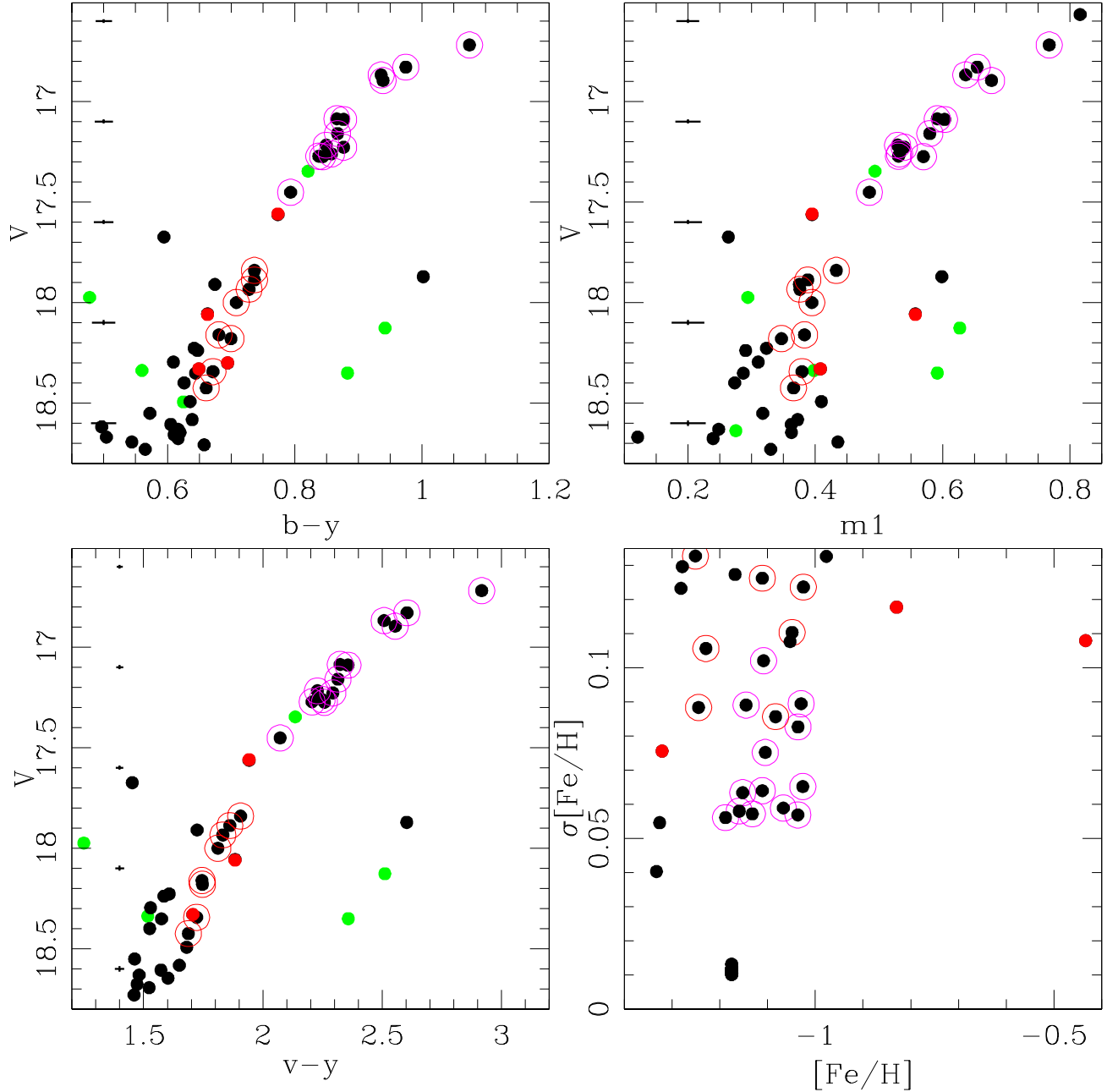


Figure 4. Same as Fig. 1 for Lindsay 1.

Harris, W. E. 1996, *AJ*, 112, 1487, doi: [10.1086/118116](https://doi.org/10.1086/118116)

Hauck, B., & Mermilliod, M. 1998, *A&AS*, 129, 431, doi: [10.1051/aas:1998195](https://doi.org/10.1051/aas:1998195)

Hill, A., & Zaritsky, D. 2006, *AJ*, 131, 414, doi: [10.1086/498647](https://doi.org/10.1086/498647)

Hollyhead, K., Kacharov, N., Lardo, C., et al. 2017, *MNRAS*, 465, L39, doi: [10.1093/mnrasl/slw179](https://doi.org/10.1093/mnrasl/slw179)

Hollyhead, K., Lardo, C., Kacharov, N., et al. 2018, *MNRAS*, 476, 114, doi: [10.1093/mnras/sty230](https://doi.org/10.1093/mnras/sty230)

Johnson, C. I., Rich, R. M., Pilachowski, C. A., et al. 2015, *AJ*, 150, 63, doi: [10.1088/0004-6256/150/2/63](https://doi.org/10.1088/0004-6256/150/2/63)

Kayser, A., Hilker, M., Grebel, E. K., & Willemsen, P. G. 2008, *A&A*, 486, 437, doi: [10.1051/0004-6361:200809446](https://doi.org/10.1051/0004-6361:200809446)

Kim, J. J., & Lee, Y.-W. 2018, ArXiv e-prints. <https://arxiv.org/abs/1807.01317>

Lim, D., Hong, S., & Lee, Y.-W. 2017, *ApJ*, 844, 14, doi: [10.3847/1538-4357/aa79aa](https://doi.org/10.3847/1538-4357/aa79aa)

Marino, A. F., Milone, A. P., Karakas, A. I., et al. 2015, *MNRAS*, 450, 815, doi: [10.1093/mnras/stv420](https://doi.org/10.1093/mnras/stv420)

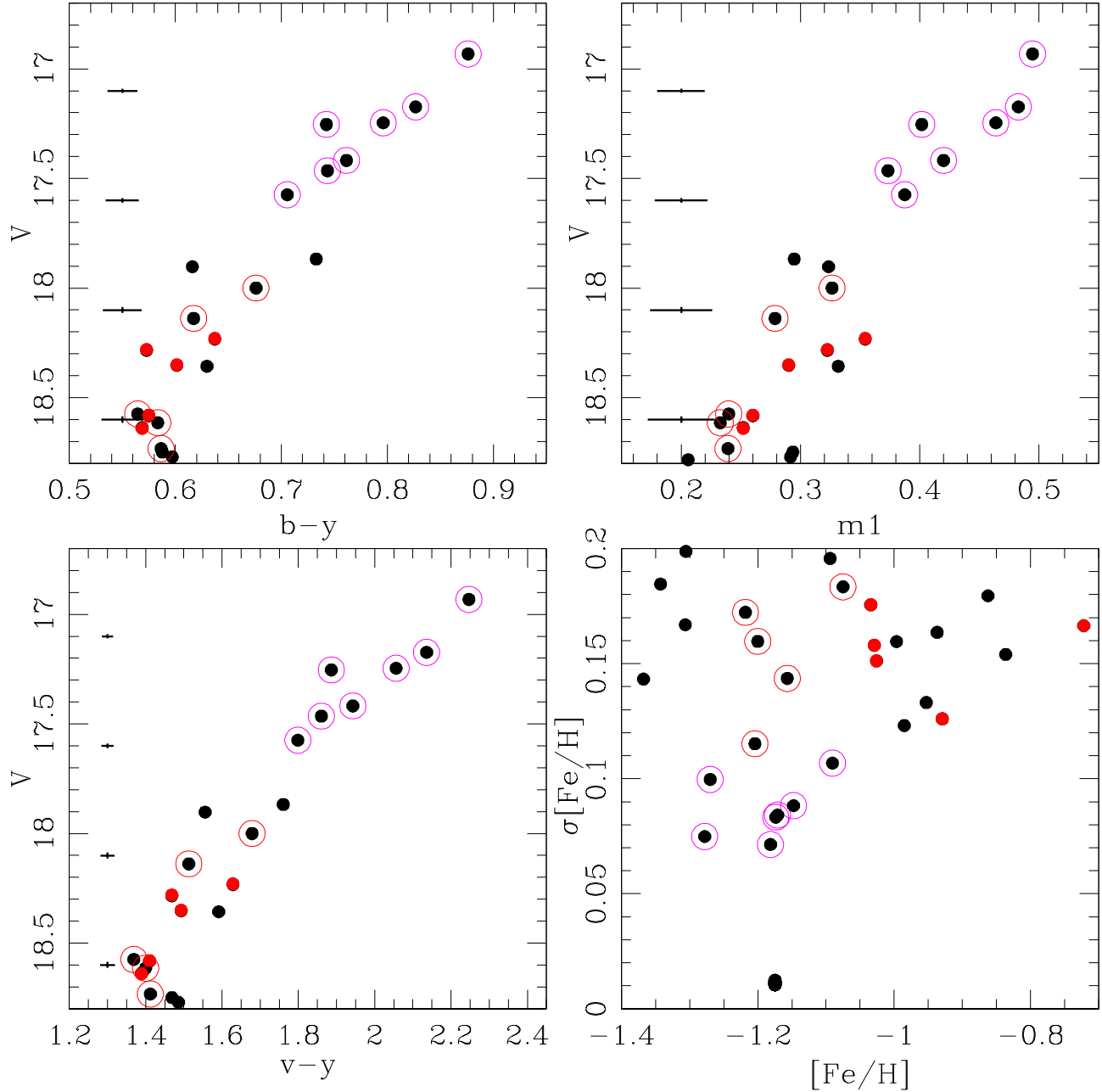


Figure 5. Same as Fig. 1 for Lindsay 113.

Martell, S. L., & Grebel, E. K. 2010, *A&A*, 519, A14,
doi: [10.1051/0004-6361/201014135](https://doi.org/10.1051/0004-6361/201014135)

Massari, D., Lapenna, E., Bragaglia, A., et al. 2016,
MNRAS, 458, 4162, doi: [10.1093/mnras/stw583](https://doi.org/10.1093/mnras/stw583)

McLaughlin, D. E., & van der Marel, R. P. 2005a, *ApJS*,
161, 304, doi: [10.1086/497429](https://doi.org/10.1086/497429)

—. 2005b, *ApJS*, 161, 304, doi: [10.1086/497429](https://doi.org/10.1086/497429)

Mighell, K. J., Sarajedini, A., & French, R. S. 1998, *AJ*,
116, 2395, doi: [10.1086/300591](https://doi.org/10.1086/300591)

Mucciarelli, A., Origlia, L., Ferraro, F. R., & Pancino, E.
2009a, *ApJL*, 695, L134,

doi: [10.1088/0004-637X/695/2/L134](https://doi.org/10.1088/0004-637X/695/2/L134)

Mucciarelli, A., Origlia, L., Maraston, C., & Ferraro, F. R.
2009b, *ApJ*, 690, 288, doi: [10.1088/0004-637X/690/1/288](https://doi.org/10.1088/0004-637X/690/1/288)

Niederhofer, F., Bastian, N., Kozhurina-Platais, V., et al.
2017, *MNRAS*, 465, 4159, doi: [10.1093/mnras/stw3084](https://doi.org/10.1093/mnras/stw3084)

Osborn, W. 1971, *The Observatory*, 91, 223

Paunzen, E. 2015, *A&A*, 580, A23,
doi: [10.1051/0004-6361/201526413](https://doi.org/10.1051/0004-6361/201526413)

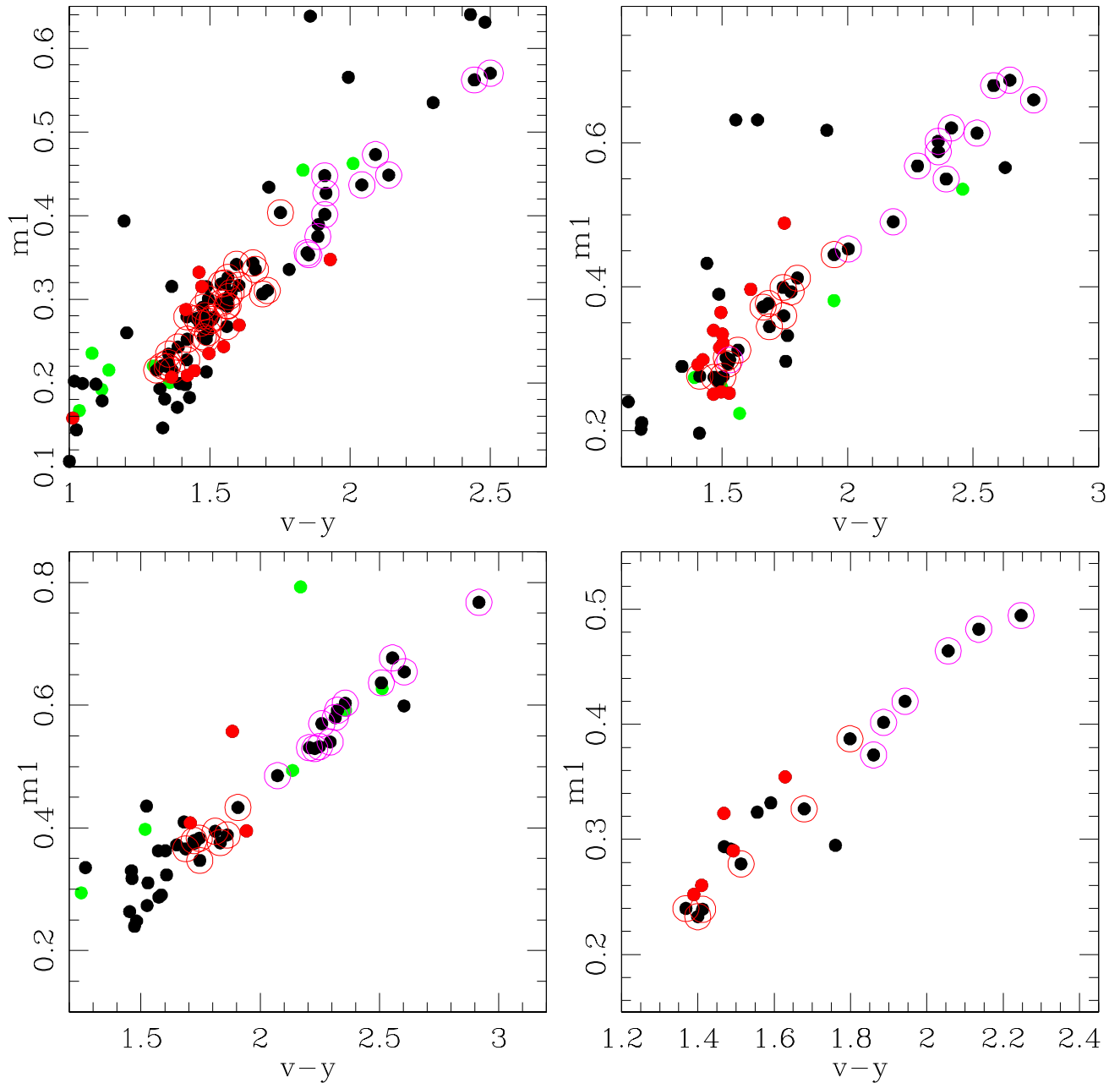


Figure 6. $v - y$ versus m_1 color-color diagrams of NGC 339 (upper-left), NGC 361 (upper-right), Lindsay 1 (bottom-left), and Lindsay 113 (bottom-right), respectively. Symbols as are in Fig. 1.

Piatti, A. E. 2011a, MNRAS, 416, L89,

doi: [10.1111/j.1745-3933.2011.01105.x](https://doi.org/10.1111/j.1745-3933.2011.01105.x)

— 2011b, MNRAS, 418, L69,

doi: [10.1111/j.1745-3933.2011.01145.x](https://doi.org/10.1111/j.1745-3933.2011.01145.x)

— 2012, ApJL, 756, L32,

doi: [10.1088/2041-8205/756/2/L32](https://doi.org/10.1088/2041-8205/756/2/L32)

Piatti, A. E., & Koch, A. 2018, ApJ, submitted.

Piatti, A. E., Santos, J. F. C., Clariá, J. J., et al. 2001,

MNRAS, 325, 792, doi: [10.1046/j.1365-8711.2001.04503.x](https://doi.org/10.1046/j.1365-8711.2001.04503.x)

Piatti, A. E., Sarajedini, A., Geisler, D., Gallart, C., &

Wischnjewsky, M. 2007, MNRAS, 381, L84,

doi: [10.1111/j.1745-3933.2007.00373.x](https://doi.org/10.1111/j.1745-3933.2007.00373.x)

Pryor, C., & Meylan, G. 1993, in Astronomical Society of the Pacific Conference Series, Vol. 50, Structure and

Dynamics of Globular Clusters, ed. S. G. Djorgovski &

G. Meylan, 357

Simpson, J. D., De Silva, G., Martell, S. L., Navin, C. A., & Zucker, D. B. 2017, *MNRAS*, 472, 2856, doi: [10.1093/mnras/stx2174](https://doi.org/10.1093/mnras/stx2174)

Stetson, P. B., Davis, L. E., & Crabtree, D. R. 1990, in *Astronomical Society of the Pacific Conference Series*, Vol. 8, *CCDs in astronomy*, ed. G. H. Jacoby, 289–304

Walker, M. G., Mateo, M., Olszewski, E. W., et al. 2006, *AJ*, 131, 2114, doi: [10.1086/500193](https://doi.org/10.1086/500193)

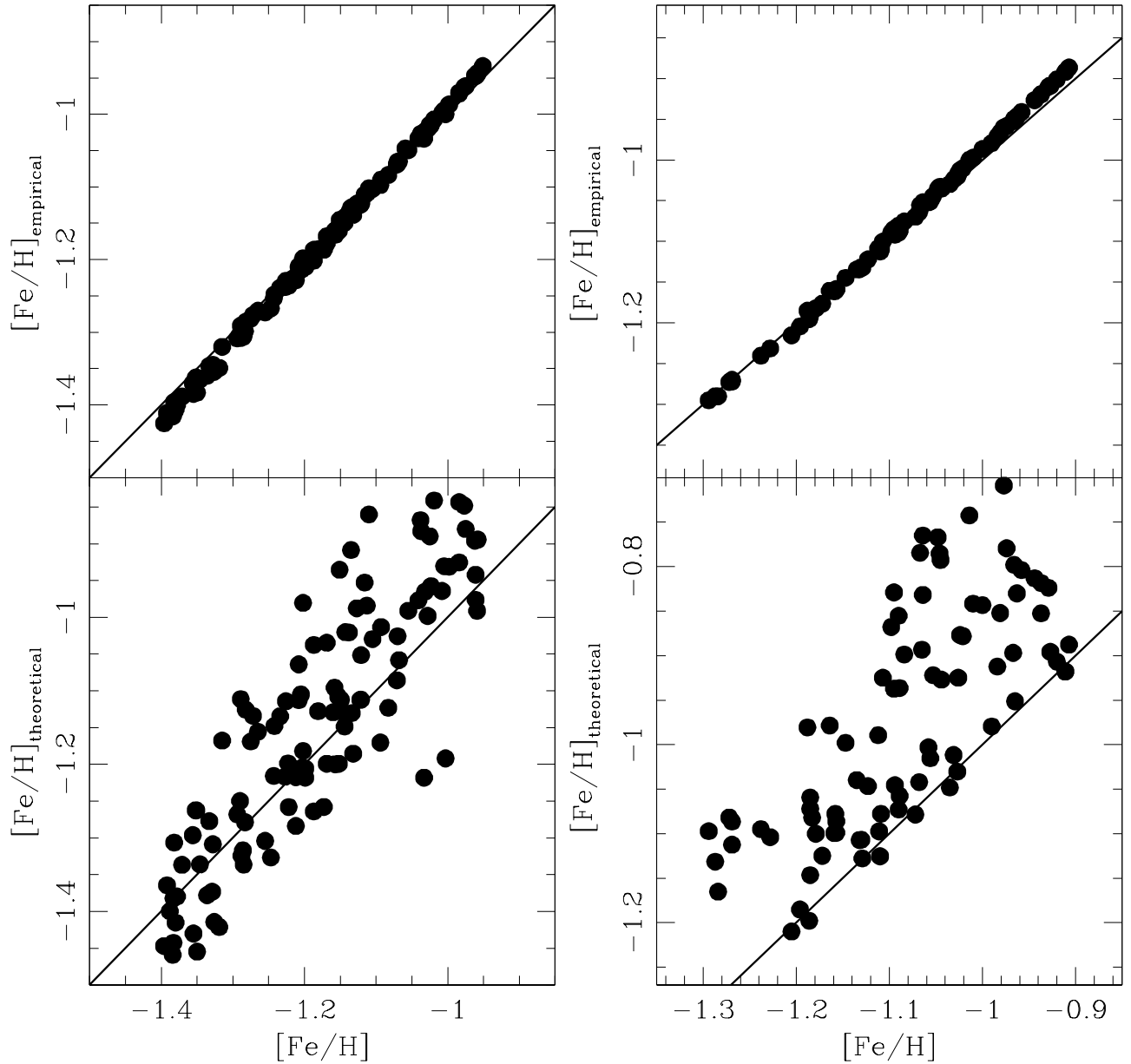


Figure 7. $[\text{Fe}/\text{H}]$ values derived from the semi-empirical calibration of Calamida et al. (2007) compared with those based on the empirical (top) and theoretical (bottom) calibrations, for NGC 339 (left) and NGC 361 (right). The solid line represents the identity relationship.

APPENDIX

A. $[\text{Fe}/\text{H}]$ VALUES BASED ON CALAMIDA ET AL (2007)'S CALIBRATIONS.

For the sake of the reader, we present here a comparison between metallicities derived from different Calamida et al. (2007)'s calibrations, namely: empirical, theoretical and semi-empirical ones. As can be seen in Figs. 7 and 8, metallicities derived with the empirical or semi-empirical calibrations agree quite well, and the present results would not change if a different calibration were used to estimate the star metal abundances. The theoretical calibration underestimates metallicities by ~ 0.2 dex, in particular in the intermediate metallicity range of the considered clusters, as shown by Calamida et al. (2007).

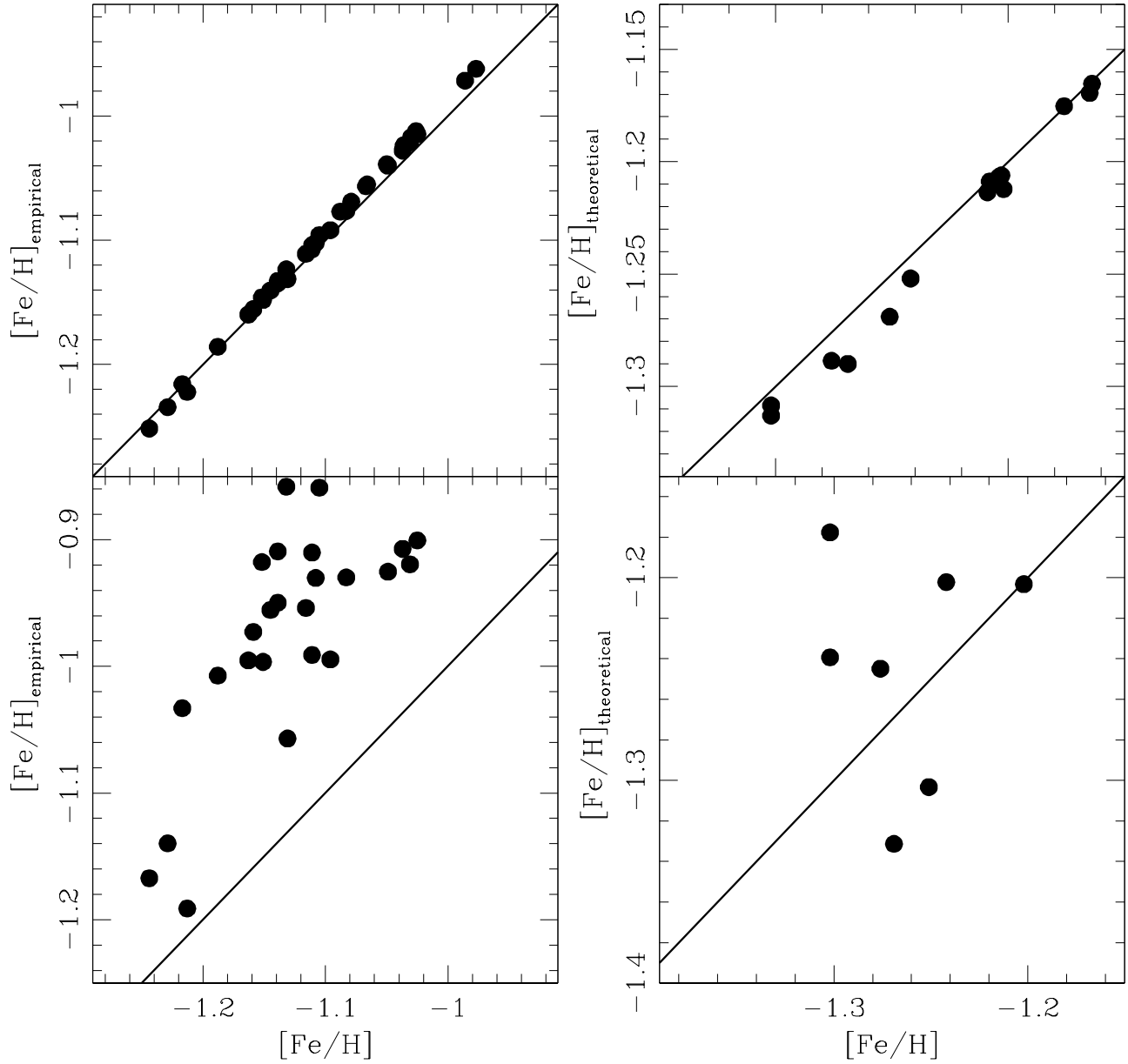


Figure 8. $[\text{Fe}/\text{H}]$ values derived from the semi-empirical calibration of Calamida et al. (2007) compared with those based on the empirical (top) and theoretical (bottom) calibrations, for L1 (left) and L113 (right). The solid line represents the identity relationship.